

# Molecular PET/CT mapping of rhACE2 distribution and quantification in organs to aid in SARS-CoV-2 targeted therapy

Hua Zhu<sup>1</sup>, Zilei Wang<sup>2</sup>, Chuanke Zhao<sup>1</sup>, Chuangui Li<sup>3</sup>, Song Liu<sup>1</sup>, Jin Ding<sup>1</sup>, Chengxue He<sup>1</sup>, Jiayue Liu<sup>1</sup>, Bin Dong<sup>1</sup>, Zhi Yang<sup>1</sup>, Qi Liu<sup>4</sup>, and Youping Liu<sup>2</sup>

<sup>1</sup>Beijing Cancer Hospital

<sup>2</sup>Southwest Medical University

<sup>3</sup>The First Affiliated Hospital of Hebei North University

<sup>4</sup>Peking University Shenzhen Graduate School

May 8, 2023

## Abstract

**Objectives** The aim of this study was to assess the potential of noninvasive and repeated monitoring of rhACE2 distribution and content in organs using the ACE2-specific nuclide probe <sup>68</sup>Ga-HZ20. **Methods** We optimized the labeling conditions of the probe and evaluated its safety. A mouse organ *in situ* rhACE2 high-aggregation model was constructed for the first time, and *in vivo* real-time PET imaging of rhACE2 was performed using the ACE2-specific PET agent <sup>68</sup>Ga-HZ20. The distribution and uptake of the probe were analyzed, and the model was validated. **Results** This radiotracer exhibited reliable radiochemical properties *in vitro* and maintained a high affinity for rhACE2 *in vivo*. In terms of probe uptake, <sup>68</sup>Ga-HZ20 showed a good target-to-nontarget ratio, and the correlation between the uptake value of the probe and the dose of rhACE2 was >90% in both models; the probe was rapidly cleared from the circulatory system and excreted by the kidneys and urinary system. No organs were damaged after the injection of high doses of probe. **Conclusions** This technology for noninvasively and repeatedly monitoring the content and distribution of rhACE2 *in vivo* aids in clarifying the resident capacity of rhACE2 in organs and in analyzing the preventive effect of rhACE2 against SARS-CoV-2 and the effectiveness of therapies for COVID-19.

## Molecular PET/CT mapping of rhACE2 distribution and quantification in organs to aid in SARS-CoV-2 targeted therapy

Zilei Wang<sup>1,2,+</sup>, Chuanke Zhao<sup>3,+</sup>, Chuangui Li<sup>4,+</sup>, Song Liu<sup>2</sup>, Jin Ding<sup>2</sup>, Chengxue He<sup>2</sup>, Jiayue Liu<sup>2</sup>, Bin Dong<sup>5</sup>, Zhi Yang<sup>2,6</sup>, Qi Liu<sup>6,\*</sup>, Hua Zhu<sup>2,6\*</sup>, Youping Liu<sup>1,\*</sup>

## Affiliations

<sup>1</sup> School of Basic Medical Science, Southwest Medical University, Luzhou 646000, China.

<sup>2</sup> Key Laboratory of Carcinogenesis and Translational Research (Ministry of Education/Beijing), Key Laboratory for Research and Evaluation of Radiopharmaceuticals (National Medical Product Administration), Department of Nuclear Medicine, Peking University Cancer Hospital & Institute, Beijing 100142, China.

<sup>3</sup> Key Laboratory of Carcinogenesis and Translational Research (Ministry of Education/Beijing), Department of Biochemistry and Molecular Biology, Peking University Cancer Hospital and Institute, Beijing 100142, China.

<sup>4</sup> Department of Nuclear Medicine, First Affiliated Hospital of Hebei North University, Zhangjiakou 075000, China.

<sup>5</sup> Central Laboratory, Peking University Cancer Hospital and Institute, Beijing 100142, China.

<sup>6</sup> Institute of Biomedical Engineering, Peking University Shenzhen Graduate School, Shenzhen, Guangdong 518055, China.

Correspondence should be addressed:

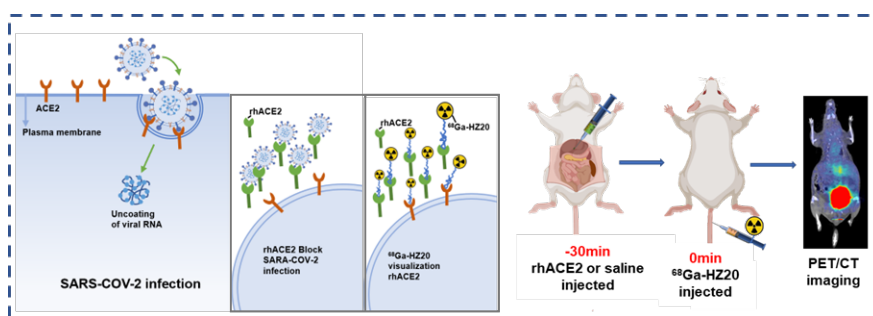
**Youping Liu** : School of Basic Medical Science, Southwest Medical University, Luzhou 646000, China; Tel.: +86 0830 3160073; email: [lyp2507622@163.com](mailto:lyp2507622@163.com)

**Hua Zhu** : Key Laboratory of Carcinogenesis and Translational Research (Ministry of Education/Beijing), Key Laboratory for Research and Evaluation of Radiopharmaceuticals (National Medical Product Administration), Department of Nuclear Medicine, Peking University Cancer Hospital & Institute, Beijing 100142, China and Institute of Biomedical Engineering, Peking University Shenzhen Graduate School, Shenzhen, Guangdong 518055, China; Tel.: +86 010 88196495; email:

[zhuhuaBCH@pku.edu.cn](mailto:zhuhuaBCH@pku.edu.cn)

**Qi Liu** : Institute of Biomedical Engineering, Peking University Shenzhen Graduate School, Shenzhen, Guangdong 518055, China; Tel.: +86 0755 26038837; email: [liuqi@pkusz.edu.cn](mailto:liuqi@pkusz.edu.cn)

## Abstract



**Objectives** The aim of this study was to assess the potential of noninvasive and repeated monitoring of rhACE2 distribution and content in organs using the ACE2-specific nuclide probe  $^{68}\text{Ga}\text{-HZ20}$ .

**Methods** We optimized the labeling conditions of the probe and evaluated its safety. A mouse organ *in situ* rhACE2 high-aggregation model was constructed for the first time, and *in vivo* real-time PET imaging of rhACE2 was performed using the ACE2-specific PET agent  $^{68}\text{Ga}\text{-HZ20}$ . The distribution and uptake of the probe were analyzed, and the model was validated.

**Results** This radiotracer exhibited reliable radiochemical properties *in vitro* and maintained a high affinity for rhACE2 *in vivo*. In terms of probe uptake,  $^{68}\text{Ga}\text{-HZ20}$  showed a good target-to-nontarget ratio, and the correlation between the uptake value of the probe and the dose of rhACE2 was  $>90\%$  in both models; the probe was rapidly cleared from the circulatory system and excreted by the kidneys and urinary system. No organs were damaged after the injection of high doses of probe.

**Conclusions** This technology for noninvasively and repeatedly monitoring the content and distribution of rhACE2 *in vivo* aids in clarifying the resident capacity of rhACE2 in organs and in analyzing the preventive effect of rhACE2 against SARS-CoV-2 and the effectiveness of therapies for COVID-19.

**Keywords:** SARS-CoV-2, PET imaging,  $^{68}\text{Ga}\text{-HZ20}$ , rhACE2-organ model

## Introduction

Coronavirus disease 2019 (COVID-19), caused by severe acute respiratory syndrome coronavirus 2 (SARS-CoV-2), poses a significant threat to public health and a great burden on the global economy<sup>1</sup>. SARS-CoV-2 and severe acute respiratory syndrome coronavirus (SARS-CoV) have 79.5% homologous sequences, and

their S protein has 76.5% similarity in amino acid sequences<sup>2</sup>. Based on previous studies, researchers quickly identified angiotensin-converting enzyme 2 (ACE2) as a key receptor for SARS-CoV-2<sup>1,3-5</sup>. ACE2 plays a key negative regulatory role in the renin-angiotensin system (RAS)<sup>6,7</sup> and promotes amino acid transport in the kidney and intestine under normal physiological conditions<sup>5</sup>. ACE2 is essential for SARS-CoV-2 to invade human cells, and during infection, the receptor-binding domain (RBD) on the S1 subunit of SARS-CoV-2 binds to ACE2, which then fuses the cell membrane of the virus to the host cell, thereby mediating viral entry into the host cell<sup>8</sup>. However, ACE2 deficiency may aggravate the prognosis of patients with COVID-19<sup>9</sup>, especially those with underlying diseases (such as hypertension, heart disease, cirrhosis and cancer)<sup>10,11</sup>.

Blocking spike/ACE2 conjugation is a central strategy for vaccine design and multiple therapeutics<sup>12</sup>. With the development of drugs for managing COVID-19, patient outcomes have improved significantly. However, in some elderly people with underlying diseases, SARS-CoV-2 continues to pose a severe threat; additionally, herd immunity is low, it is difficult to produce an effective response to the vaccine, and the neutralization effect of monoclonal antibodies is hindered because SARS-CoV-2 hides its RBD after infection in the body<sup>13-16</sup>. Moreover, as the virus evolves, variants continue to emerge, which not only affects the infectivity of SARS-CoV-2 but also reduces the efficacy of vaccines, convalescent serum, and monoclonal antibody therapy<sup>17-21</sup>. Therefore, ACE2 is an excellent drug target because regardless of the number of SARS-CoV-2 variants, the virus relies on ACE2 to infect humans<sup>2,22</sup>.

Recombinant human ACE2 (rhACE2) can be used as a supplement to ACE2 in the body, which can competitively block SARS-CoV-2 infection<sup>23,24</sup>. Preclinical research has revealed that rhACE2 protects mice from severe acute lung injury by inhibiting the binding of SARS coronavirus to its own ACE2 in lung cells<sup>1,25</sup> and that rhACE2 can inhibit SARS-CoV-2 infection in artificial human tissues<sup>26</sup>. Clinical trials (NCT04335136) have demonstrated that soluble rhACE2 (APN01) binds to the RBD and full-length spike protein of the SARS-CoV-2 variant and is effective in neutralizing infection in all test variants<sup>27</sup>. Furthermore, another study obtained good results in animal experiments by *in situ* administration of APN01 in the respiratory tract in the form of aerosol inhalation, and a phase I clinical trial (NCT05065645) is currently ongoing<sup>28</sup>. Nevertheless, a clinical trial to assess the efficacy of rhACE2 in COVID-19 patients in China (NCT04287686) was withdrawn<sup>29</sup> due to concerns that ACE2 infusion may reduce circulating Ang II and increase Ang-(1-7) levels, leading to possible complications such as hypotension in patients with COVID-19 in the late stages of the disease<sup>30</sup>. Our current study may alleviate this concern, as we can accurately reflect *in situ* ACE2 levels in organs through PET imaging, which can help in evaluating the efficacy of rhACE2 and provide a scientific basis for rhACE2 therapy.

Existing methods such as immunohistochemistry and serological testing cannot be used to detect the dynamic expression level of ACE2 and its spatial distribution *in vivo*, which is an obstacle to further development of ACE2 as a biomarker for the diagnosis and treatment of COVID-19. Molecular imaging, as a noninvasive method, can be used to quantitatively monitor the spatial distribution of molecular targets *in vivo* with high sensitivity. Positron emission tomography (PET) has been widely used to detect disease-related biomarkers using radioligands.

DX600 is an ACE2-specific inhibitory peptide found in the peptide library based on restriction phages with a  $K_i$  as low as 2.8 nM and is highly specific for ACE2<sup>31</sup>. For radionuclide<sup>68</sup>Ga labeling, we coupled DX600 with the bifunctional chelate DOTA, named HZ20. In our previous study<sup>32</sup>, HZ20 was shown to target rhACE2 with high affinity and specificity, and the  $K_d$  values of the SPR assay for DX600 and HZ20 were 98.7 and 100.0 nM, respectively. Additionally, we used <sup>68</sup>Ga-HZ20 to assess the background level of ACE2 and the *in vivo* distribution and expression levels in 20 healthy volunteers of different ages and sexes and one COVID-19-rehabilitated person<sup>32</sup>. We also developed a neutralized nanobody-based radiotracer, <sup>68</sup>Ga-Nb1159. It can be used to visualize the localization and distribution of the SARS-CoV-2 RBD with a high target-to-background ratio<sup>33</sup>. Furthermore, there have been no reports of radiotracer detection of the distribution and content of rhACE2 in different organs.

Inspired by the previous ACE2/RBD targeting probes and the recent eased restrictions, we aimed to noninvasively map rhACE2 in the body in various tissue microenvironments. We optimized the labeling conditions

of radionuclide  $^{68}\text{Ga}$  and obtained the radioactive probe  $^{68}\text{Ga}$ -HZ20 with a higher labeling rate and yield. We also constructed rhACE2 *in situ* models in different organs of mice, for example, liver, spleen, brain and tumor tissues, and used  $^{68}\text{Ga}$ -HZ20 to monitor the content and distribution of exogenous rhACE2 *in situ* in model mouse organs for rhACE2 therapy.

## Materials and Methods

**General Procedures:** All solvents and chemicals were purchased from reagent vendors and no purification was performed prior to use. HZ20 were custom synthesized by ChinaPeptides Co., Ltd (Shanghai, China) or CSBio (San Diego, California). Sep-Pak Accell Plus QMA and Sep-Pak C18-Light cartridges were purchased from Waters (Ireland). Acrodisc 25 mm syringe filter (0.22  $\mu\text{m}$ ) was purchased from Pall Corporation (USA). The labeling yield, radiochemical purity and stability were analyzed by radio-high performance liquid chromatography (HPLC) (1200, Agilent, USA) equipped with  $\gamma$  detector (Flow-count, Bioscan, Washington, D.C., USA), using a C18 column (Eclipse Plus C18, 4.5  $\times$  250 mm, 5 $\mu\text{m}$ , Agilent, USA). The Micro-PET/CT imaging studies of small animals were performed on the Micro-PET/CT of PINGSENG Healthcare Inc (Shanghai, China). The  $^{68}\text{Ge}$ - $^{68}\text{Ga}$  generator was purchased from ITM Co., Ltd, Germany. rhACE2 purchased from Sydlabs (BP003061). RIPA lysate purchased from Solarbio (R0010).

**The Radiolabeling and quality control of  $^{68}\text{Ga}$ -HZ20 were conducted as previously reported procedures with some modifications** [Supplemental Information].

### rhACE2 administrations in KM mice

For subcutaneous-rhACE2 and tumor rhACE2 models, different doses of rhACE2 were directly injected into the corresponding positions 30 min before PET imaging; For the *in situ* rhACE2-intraperitoneal liver or -spleen model, after anesthetizing mice with 1.25% tribromoethanol at 0.2 ml/10g 30 min in advance, the target organ was exposed after opening the abdomen, and different contents of rhACE2 were injected using insulin needles, and the injection volume was not more than 50 $\mu\text{L}$ ; The anterior fontanelle is the origin, 1.7 mm on the right, 0.7 mm anteriorly, and 3 mm deep for fixed-point injection of the right caudate nucleus.

### Micro-PET/CT imaging of mice model

7.4 MBq/200 $\mu\text{L}$   $^{68}\text{Ga}$ -HZ20 was injected into model mice through the tail vein, anesthetized with isoflurane (2-3%, 1 L/min oxygen), and placed on a heated bed for Micro-PET/CT imaging scanner to statically acquire PET/CT images for a certain period of time. 50-fold unlabeled HZ20 and 7.4 MBq  $^{68}\text{Ga}$ -HZ20 were co-injected into mice for blocking studies. For *ex vivo* imaging of the target tissue, the weight of the organ was weighed, and Micro-PET/CT imaging is performed directly, and the  $\gamma$ -counter assay was performed immediately following the PET imaging procedure. A region of interest (ROI) was plotted on the CT image and mapped onto the PET to further acquire its SUVmax value for further analysis.

**Western blot detection of rhACE2 protein in injection site and immunohistochemical detection of ACE2 at organ background level.**[Supplementary Materials]

### Mice organ HE staining

Normal KM mice are injected with a 37MBq  $^{68}\text{Ga}$ -HZ20 probe 1 week in advance, the main organs were taken for paraffin embedding after sacrifice, after dewaxing and rehydration, 5  $\mu\text{m}$  longitudinal sections are stained with hematoxylin solution for 5 min, then differentiated (2% hydrochloric acid alcohol) for several seconds, then transferred to water, washed for 30 min and then stained with eosin solution for 1 min, then dehydrated with fractionated alcohol and cleared in xylene, sealed in neutral colloidal medium, and image scanning (Aperio Versa 200, Leica).

### Statistics

Statistical analysis was performed using Origin software (V.2022) and Prism (V7.0, GraphPad software). Organ uptake data in the form of SUVmax were grouped by time. To compare the distribution between samples, parametric continuous variables were expressed as mean  $\pm$  SD. Unpaired t-tests for independent

samples were used to compare SUVmax values between groups. P-values less than 0.05 were considered significant.

## Results

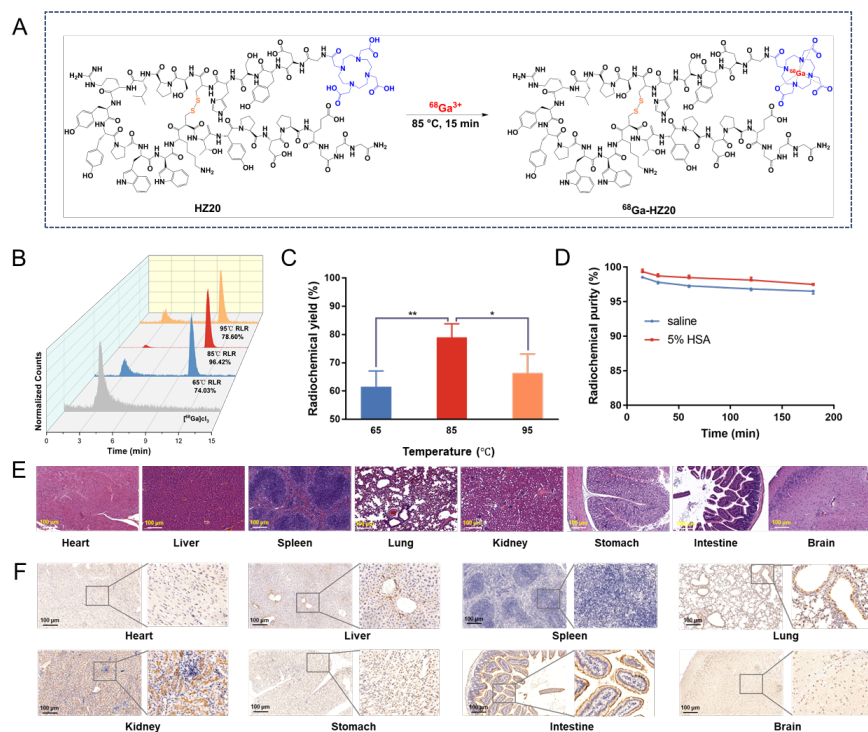


Figure 1. In vitro characterization and safety assessment of  $^{68}\text{Ga}$ -HZ20. (A) Schematic illustration of the synthesis of the  $^{68}\text{Ga}$ -HZ20 probe. (B) Radiolabeling rate (RLR) of  $^{68}\text{Ga}$ -HZ20 at different temperatures. (C) Radiochemical yield of  $^{68}\text{Ga}$ -HZ20 at different temperatures (n=3). (D) Stability analysis of  $^{68}\text{Ga}$ -HZ20 over time in saline and 5% HSA at 37 (n=3). (E) HE staining of major organs indicates the safety of radio-tracer (n=5). (F) IHC of ACE2 expression levels in major organs.

### *In vitro* characterization and safety assessment of $^{68}\text{Ga}$ -HZ20

The procedure of  $^{68}\text{Ga}$ -HZ20 radiosynthesis is shown in Fig. 1A. Radio-HPLC showed nondecayed radiolabeling rates at 65 °C, 85 °C, and 95 °C of 74.03%, 96.42%, and 78.60% for the  $^{68}\text{Ga}$ -HZ20 probe, respectively (Fig. 1B). After purification on a C18 column, the radiochemical purity was higher than 99% (Fig. S1), and the nondecayed radiochemical yields were  $61.51 \pm 4.47\%$ ,  $78.99 \pm 3.92\%$ , and  $66.34 \pm 5.51$  (n=3), respectively (Fig. 1C). The specific activity was  $(3.37 \pm 0.35) \times 10^4 \text{GBq/mmol}$  (n=3). The *in vitro* stability of the probe was tested using radio-HPLC. The radiochemical purity of  $^{68}\text{Ga}$ -HZ20 in either normal saline or 5% HSA was higher than 96% within 180 min at room temperature incubation (n=3) (Fig. 1D). To evaluate the safety of the probe,  $^{68}\text{Ga}$ -HZ20 of 37 MBq was injected into KM mice (n=5) one week in advance, and then the main organs were sampled for HE staining; no organic damage to the organs was observed (Fig. 1E). Immunohistochemical staining was used to assess the expression level of ACE2 in the main organs of mice. Almost no expression of ACE2 was observed in the stomach, heart, or spleen (-) of mice, with microexpression visible in the brain (+). There was no expression of ACE2 in hepatocytes, and notably, it was highly expressed in the hepatic manifold (++); similarly, it was not expressed in alveolar cells but was highly expressed in bronchial epithelial cells (++) in addition, high expression was observed in both the kidneys and small intestine (++) supporting symptoms such as respiratory and fecal-oral transmission of SARS-CoV-2 as well as acute kidney injury and diarrhea following infection (Fig. 1F).

## Micro-PET/CT studies of the $^{68}\text{Ga}$ -HZ20 probe in normal mice

PET images of normal KM mice showed that the probe entered the body and was rapidly distributed with blood circulation and metabolized by the kidney and bladder (Fig. S2A). The maximum single-voxel standardized uptake value (SUVmax), which is the standard nuclear medicine metric, was chosen to show the probe accumulation in tissues or organs by measuring the maximum voxel value in a volume of interest (organs) standardized to patient mass and administered activity. The SUVmax showed that the probe was rapidly cleared from the mouse heart blood pool from  $0.51\pm 0.04$  to  $0.15\pm 0.04$  ( $p=0.0004$ ) at 60 min after injection, and the remaining probe mainly accumulated in the kidneys at  $1.3\pm 0.16$  (Fig. S2B). Although the uptake values of the liver ( $0.43\pm 0.02$ ) and lungs ( $0.43\pm 0.03$ ) were similar, the density in the liver was much greater than that in the lungs, suggesting that the uptake of probe was higher in lung tissue than in liver tissue.

## Micro-PET study of $^{68}\text{Ga}$ -HZ20 in the rhACE2-subcutaneous model

In KM model mice, different doses (0.1, 0.2, 0.4 and 0.8 nmol) of commercial rhACE2 protein were injected into the right shoulder. The molecular weight of the rhACE2 protein was approximately 100 kDa according to mass spectrometry (Fig. S3). PET imaging showed that  $^{68}\text{Ga}$ -HZ20 had high specificity and sensitivity for rhACE2 *in vivo* (Fig. 2A, Fig. S4). This probe can locate regions with rhACE2 aggregation and reveal the distribution of rhACE2. Compared to the contralateral side injected with saline control, micro-PET/CT imaging clearly showed the specific uptake of the probe at the rhACE2 injection site, and the uptake rate increased with the rhACE2 injection dose. Similarly, at the same time point after probe injection, SUVmax also increased with the amount of rhACE2 (0.1, 0.2, 0.4 and 0.8 nmol). Furthermore, in the 0.4 nmol and 0.8 nmol rhACE2 injection groups, probe uptake increased over time, reaching a maximum at 120 min after injection ( $1.70\pm 0.08$ ,  $3.13\pm 0.07$ ) and then slowly decreasing (Fig. 2C). The ratio of target site to muscle for response probe targeting and specificity also increased with increasing rhACE2 injection to  $2.50\pm 0.41$ ,  $8.24\pm 0.47$ ,  $15.57\pm 0.49$ , and  $25.45\pm 1.48$ , respectively, at 240 min (Fig. 2D). Once PET image acquisition was complete, the rhACE2 (0.2 nmol, 0.4 nmol) injection site and the main organs were sampled for *ex vivo* imaging (Fig. 2E), and the results showed significant dose-dependent uptake of the probe at the rhACE2 injection site. High uptake was detected in the kidneys, but there was almost no uptake in other normal organs. The correlation between SUVmax and rhACE2 dose was analyzed 120 min after injection, and the  $R^2$  was 0.9914 (Fig. 2F). We selected the 0.4 nmol rhACE2 group for a 14.63 nmol HZ20 peptide blockade study, and the uptake of probe at the rhACE2 injection site in the blockade group was significantly reduced (Fig. 2B, Fig. S5). At all time points, there was a considerable difference between the SUVmax of the HZ20 block group and that of the non-block group, which was  $1.70\pm 0.08$  compared to  $0.40\pm 0.01$  ( $p<0.0001$ ) at 120 min (Fig. 2G). After micro-PET imaging, rhACE2 residence was verified by western blotting, and the results showed that the rhACE2 protein was successfully localized at the subcutaneous injection site and remained stable *in vivo* within 240 min (Fig. 2H).

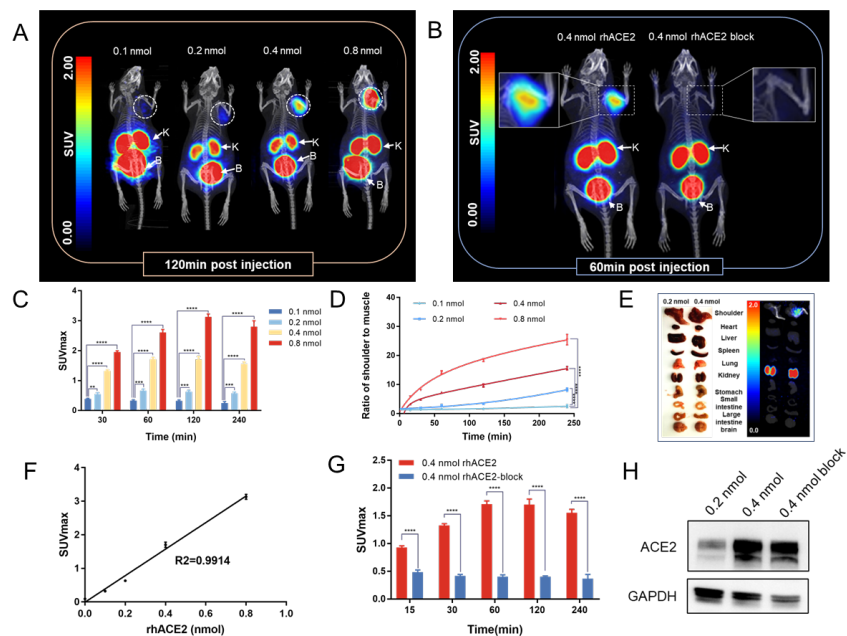


Figure 2. Evaluation of  $^{68}\text{Ga}$ -HZ20 in the rhACE2-subcutaneous models. (A) PET imaging with  $^{68}\text{Ga}$ -HZ20 in the KM mice model with subcutaneous injection of different doses of rhACE2. The white circle indicates the injection site of rhACE2. (K, B stands for kidney and bladder). (B) PET imaging of mice treated with 0.4 nmol rhACE2 and without or with 50  $\mu\text{g}$  HZ20 blocking. The white box indicates the injection site of rhACE2. (K, B stands for kidney and bladder). (C) Comparison of SUVmax at the rhACE2 injection site in Figure 2A and Figure S4. (D) The ratio of shoulder to muscle SUVmax. (E) *ex vivo* imaging of the injection site and major organs. (F) Correlation analysis between SUVmax and rhACE2 doses at 120 min after injection. (G) Comparison of SUVmax in the 0.4 nmol and 0.4 nmol block groups. (H) Western blot of rhACE2 at the injection site.

### Micro-PET study of $^{68}\text{Ga}$ -HZ20 in the rhACE2 intratumoral model

Intratumoral injection of rhACE2 and micro-PET imaging in A549 tumor-bearing mice showed that  $^{68}\text{Ga}$ -HZ20 accurately tracked rhACE2 in tumors (Fig. 3A, Fig. S6). Consistent with the western blot results, no expression of ACE2 in the A549 tumor was detected by micro-PET imaging with  $^{68}\text{Ga}$ -HZ20. In contrast, the probe uptake of the rhACE2-injected group increased with increasing injection dose. Comparing SUVmax in PET imaging in different injection groups also yielded consistent results, and SUVmax at tumor sites reached  $0.3 \pm 0.08$ ,  $0.6 \pm 0.07$ ,  $0.75 \pm 0.03$  and  $0.94 \pm 0.03$ , respectively, 30 min after probe injection (Fig. 3B). To further investigate the specificity of the probe, the SUVmax ratio of tumor to muscle was analyzed, and the results showed that when the injection group was treated with the same dose of rhACE2 protein, the ratio increased with time. At all time points, the ratio correlated with the rhACE2 injection dose. At 240 min after probe injection, the ratios were  $0.88 \pm 0.54$ ,  $4.59 \pm 0.32$ ,  $6.22 \pm 1.56$ , and  $7.13 \pm 0.54$ , respectively (Fig. 3C). After 240 min of probe injection, the tumor was sampled for *ex vivo* imaging (Fig. 3D), and consistent results with those of *in vivo* imaging were observed.  $\gamma$ -counting analysis after *ex vivo* imaging of tumor tissues showed that the % ID/g of the 0.4 nmol rhACE2 injection group was up to  $1.22 \pm 0.08$ , and there were significant differences among rhACE2 doses (Fig. 3E). The correlation analysis between rhACE2 and SUVmax showed the highest correlation 30 min after probe injection, and the  $R^2$  was 0.9176 (Fig. 3F). rhACE2 protein bands were validated in the tumor after rhACE2 injection (Fig. 3G).

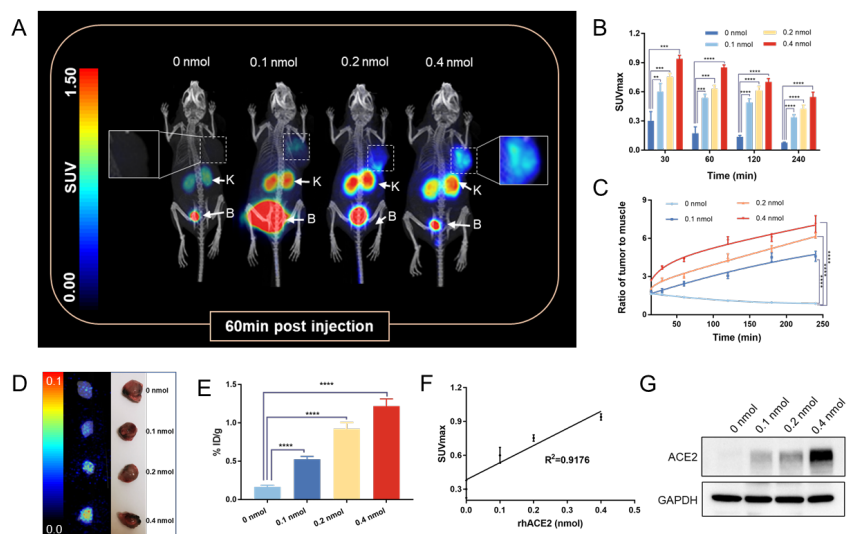


Figure 3. Evaluation of <sup>68</sup>Ga-HZ20 in the rhACE2 intratumoral model based on A549 cells. (A) PET imaging at 60 min after <sup>68</sup>Ga-HZ20 injection following intratumoral injection of different doses of rhACE2. The white box with a dashed line indicates the tumor and the injection site of rhACE2 (K, B stands for kidney and bladder). (B) Comparison of SUVmax in the tumors in Figure 3A and Figure S6. (C) The ratio of tumor to muscle SUVmax at different time points following <sup>68</sup>Ga-HZ20 injection. (D) *Ex vivo* PET imaging of tumor tissue treated with different doses of rhACE2. (E) Comparison of % ID/g in tumor tissue treated with different doses of rhACE2. (F) Correlation analysis between SUVmax and rhACE2 doses at 30 min after injection. (G) Western blot of rhACE2 at the injection site.

### Micro-PET study of <sup>68</sup>Ga-HZ20 in the rhACE2-intraperitoneal liver model

To investigate the targeting ability of the <sup>68</sup>Ga-HZ20 probe in different tissues and organs, we chose to perform PET imaging studies after *in situ* injection of different doses of rhACE2 in the liver of KM mice. PET imaging showed clear probe uptake in the liver, and the uptake was rhACE2 dose dependent (Fig. 4A, Fig. S7). Compared with the control group, the rhACE2 injection group showed a higher SUVmax value at the liver injection site, and the SUVmax obtained 15 min after probe injection was  $0.43 \pm 0.02$ ,  $0.52 \pm 0.02$  and  $0.76 \pm 0.01$ , respectively (Fig. 4B). Similarly, the target ratio of liver to muscle in the rhACE2 injection group was significantly higher than that in the blank control group, and the ratio in the 0.4 nmol rhACE2 injection group was higher than that in the 0.2 nmol rhACE2 injection group and reached the highest rate at 60 min, at  $1.3 \pm 0.20$ ,  $2.54 \pm 0.27$  and  $3.95 \pm 0.52$ , respectively (Fig. 4C). After probe injection for 150 min, the liver was sampled for  $\gamma$  counter measurement. Consistent with the PET imaging results, % ID/g in the liver also depended on rhACE2 injection doses, which were  $0.24 \pm 0.01$ ,  $0.32 \pm 0.01$ , and  $0.37 \pm 0.02$  (Fig. 4D). The correlation analysis between rhACE2 and SUVmax showed the highest correlation 60 min after injection of the probe, and the R<sup>2</sup> was 0.9994 (Fig. 4E). There was almost no expression of ACE2 in the liver tissue, but rhACE2 injection artificially increased the protein levels (Fig. 4F).

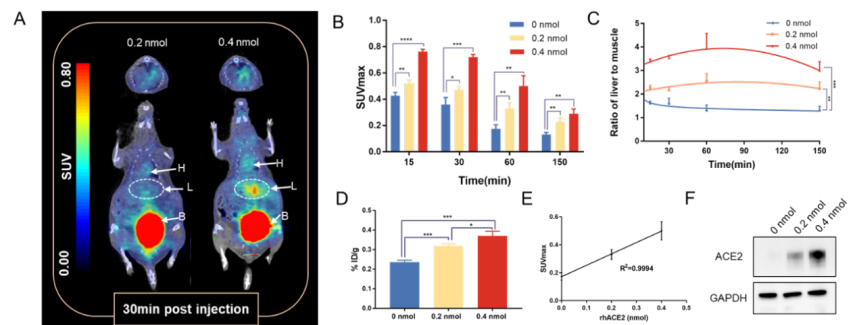


Figure 4. Evaluation of  $^{68}\text{Ga}$ -HZ20 in the rhACE2-intraperitoneal liver model. (A) PET imaging with *in situ* injection of different doses of rhACE2 in the liver. The white circle indicates the liver injection site (L, H, B stands for liver, heart and bladder). (B) Comparison of SUVmax in the liver in Figure 4A and Figure S7. (C) The ratio of liver to muscle SUVmax. (D) Comparison of liver tissue % ID/g. (E) Correlation analysis between SUVmax and rhACE2 doses at 60 min after injection. (F) Western blot of rhACE2 at the injection site.

### Micro-PET study of $^{68}\text{Ga}$ -HZ20 in the rhACE2-intraperitoneal spleen model

RhACE2 was injected *in situ* into the spleen of KM mice, and PET imaging showed significant aggregation of the  $^{68}\text{Ga}$ -HZ20 probe in the 0.4 nmol rhACE2 injection group (Fig. 5A, Fig. S7). Comparing SUVmax in PET images revealed that the difference in probe uptake in the spleen between the 0.2 nmol rhACE2 injection group and the control group was small, while that in the 0.4 nmol rhACE2 injection group was significantly higher than that of the other two groups, and the SUVmax at 15 min after probe injection was  $0.28 \pm 0.03$ ,  $0.28 \pm 0.01$  and  $0.58 \pm 0.01$ , respectively (Fig. 5B). Similarly, the splenic muscle target ratio was significantly higher in the 0.4 nmol rhACE2 injection group than in the 0.2 nmol and control groups, with 60 min ratios of  $1.25 \pm 0.20$ ,  $1.30 \pm 0.14$  and  $4.13 \pm 0.05$ , respectively (Fig. 5C). After 60 min of probe injection, the spleen was sampled for *ex vivo* imaging, and PET showed that the probe had a high uptake in the spleen in the 0.4 nmol group and a small amount of uptake in the 0.2 nmol group, especially at the injection site of rhACE2 (Fig. 5D). After *ex vivo* imaging, the spleen tissue was measured by a  $\gamma$  counter to analyze probe uptake more accurately, and the results showed that the % ID/g in the rhACE2 injection group was significantly higher than that in the control group, which was  $0.41 \pm 0.01$ ,  $0.53 \pm 0.01$  and  $0.86 \pm 0.03$ , respectively (Fig. 5E). The correlation analysis between rhACE2 and SUVmax showed the highest correlation 45 min after probe injection, and the  $R^2$  was 0.9095 (Fig. 5F). Similarly, there was almost no expression of ACE2 in the spleen, and rhACE2 aggregation in the spleen tissue was observed in the injection group, but the rhACE2 content was significantly lower than that of other model groups with the same dose, although the analysis results may be due to the small volume of the spleen and the leakage of rhACE2 during surgery (Fig. 5G).

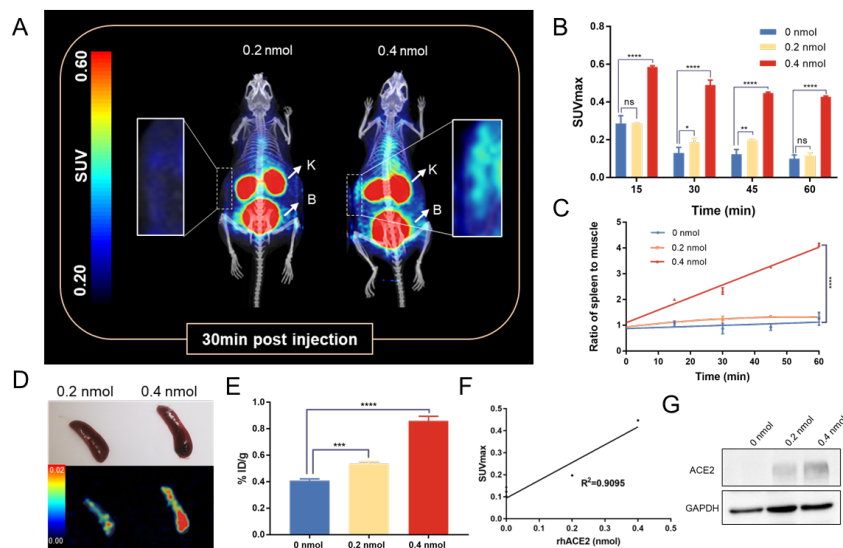


Figure 5. Evaluation of  $^{68}\text{Ga}$ -HZ20 in rhACE2-intraperitoneal spleen model. (A) PET imaging with *in situ* injection of different doses of rhACE2 in the spleen. The white box indicates the spleen injection site (K, B stands for kidney and bladder). (B) Comparison of SUVmax in the spleen in Figure 5A and Figure S8. (C) The ratio of spleen to muscle SUVmax. (D) *ex vivo* PET imaging of spleen tissue. (E) Comparison of spleen tissue % ID/g. (F) Correlation analysis between SUVmax and rhACE2 doses at 45 min after injection. (G) Western blot of rhACE2 at the injection site.

### Micro-PET study of $^{68}\text{Ga}$ -HZ20 in the rhACE2-intraperitoneal brain model

PET imaging showed slight uptake of the probe in the brains of control mice, while significant aggregation was observed in the rhACE2 injection group (Fig. 6A, Fig. S9). SUVmax showed that within 120 min after probe injection, there were significant differences between the rhACE2 injection group and the control group, and at 15 min after probe injection, the uptake values were  $0.42 \pm 0.01$ ,  $0.44 \pm 0.01$ ,  $0.56 \pm 0.02$  and  $0.72 \pm 0.01$ , respectively (Fig. 6B). The target ratio of brain to muscle also showed consistent results, with  $2.23 \pm 0.10$ ,  $2.85 \pm 0.06$ ,  $3.34 \pm 0.12$ , and  $4.23 \pm 0.12$  at 120 min, respectively (Fig. 6C). After 120 min, brain tissue *ex vivo* imaging was performed, and the results were consistent with the results of *in vivo* PET. There was almost no probe uptake in the brains of mice that were not injected with rhACE2, while the uptake of probe in brain tissue was observed in the injection group, especially in the 0.8 nmol rhACE2 group (Fig. 6D). This result also showed that the  $^{68}\text{Ga}$ -HZ20 probe can be applied to the quantitative monitoring of rhACE2 in brain tissue. Brain tissue % ID/g also showed that the rhACE2 injection group was significantly higher than that of the noninjection group, with the highest in the 0.8 nmol group, which was  $0.004 \pm 0.001$ ,  $0.024 \pm 0.001$ ,  $0.048 \pm 0.001$  and  $0.123 \pm 0.002$ , respectively (Fig. 6E). The correlation analysis between rhACE2 and SUVmax showed the highest correlation 30 min after probe injection, and the  $R^2$  was 0.9913 (Fig. 6F). The content of rhACE2 in brain tissue was detected by western blot, and the results showed that there was a small amount of ACE2 expression in the brain tissue itself, and obvious bands and gradient relationships were visible in the injection group, indicating that rhACE2 maintained stability in structure and quantity in the brain within 120 min (Fig. 6G).

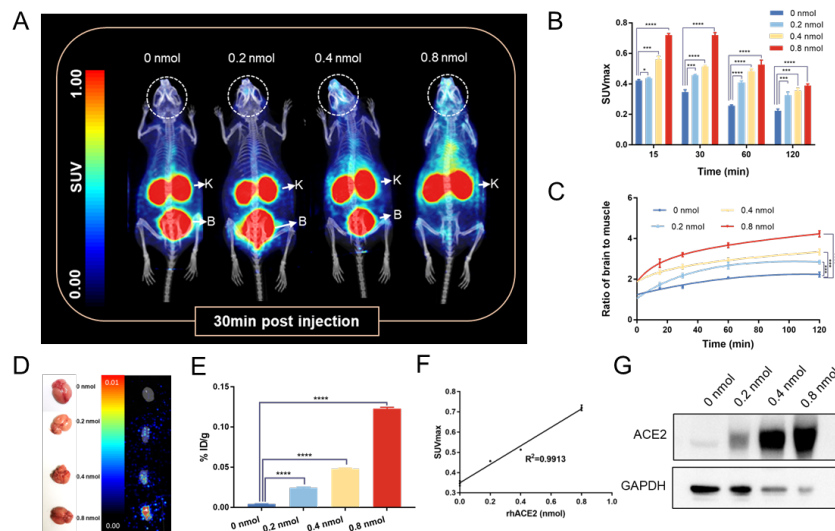


Figure 6. Evaluation of  $^{68}\text{Ga}$ -HZ20 in rhACE2- intraperitoneal brain model. (A) PET imaging with *in situ* injection of different doses of rhACE2 in the brain. The white circle indicates the brain injection site (K, B stands for kidney and bladder). (B) Comparison of SUVmax in the brain in Figure 6A and Figure S9. (C) The ratio of brain to muscle SUVmax. (D) *ex vivo* PET imaging of brain tissue (E) Comparison of brain tissue % ID/g. (F) Correlation analysis between SUVmax and rhACE2 doses at 30 min after injection. (G) Western blot of rhACE2 at the injection site.

## Discussion

According to the Johns Hopkins Center for Health Security, as of December 20, 2022, there were 650 million cumulative COVID-19 cases and 6.65 million deaths worldwide. As a functional receptor of SARS-CoV-2, ACE2 plays a great role in viral infection and prognosis *in vivo* and has thereby gained widespread attention.

The main ACE2 detection assay relies on IHC staining, which is invasive and relies heavily on experienced physicians; unfortunately, its inability to comprehensively probe lesions throughout the body limits its wider application. Nuclear medicine molecular probes can be used in noninvasive imaging of critical molecules in the human body and thus may provide a valuable tool in ACE2 examination.

Here, we described a novel ACE2-specific nuclide molecular probe,  $^{68}\text{Ga}$ -HZ20, which can be used to detect the distribution and content of rhACE2 *in vivo*. In a previous study, we performed the first quantitative analysis of ACE2 expression in human organs by PET/CT imaging using the  $^{68}\text{Ga}$ -HZ20 probe, which contributed to the understanding of the pathogenesis of SARS-CoV-2, the severity and duration of symptoms after infection, etc.<sup>32</sup>. In this study, HZ20, a specific inhibitory peptide with high affinity for ACE2, was selected as the PET imaging agent. Micro-PET/CT images of the  $^{68}\text{Ga}$ -HZ20 probe in normal KM mice showed that it had ideal pharmacokinetic characteristics and low uptake in background organs, and the probe was mainly metabolized by the kidney through the bladder. This is consistent with the abundant expression of ACE2 in the kidney, as shown by IHC. After evaluating the safety of the probe, we built subcutaneous and organ intraperitoneal *in situ* injection models of rhACE2 for research. To fully evaluate the sensitivity of the probe, we injected different doses of rhACE2 into each model. The results showed that the uptake of the probe was highly positively correlated with the content of rhACE2. To evaluate the specificity of the probe, we also conducted a blocking study in which excessive non- $^{68}\text{Ga}$ -labeled HZ20 could competitively bind to rhACE2 *in vivo*, demonstrating the specificity of the probe against rhACE2.

The latest study published in *Nature* shows that ursodeoxycholic acid (UDCA), a drug for treating liver

disease, can block the ACE2 receptor and thus viral entry into host cells, and because the drug targets host cells rather than the virus, it may prevent infection with future new variants of the virus as well as other coronaviruses that may emerge<sup>34</sup>. As rhACE2 therapy may become a preventive and therapeutic modality for critically ill COVID-19 patients<sup>23</sup>, monitoring exogenous rhACE2 is indispensable. The use of nuclear medicine molecular probes and PET imaging technology to monitor the content and distribution of rhACE2 *in vivo*, noninvasively and repeatedly, helps to clarify the mechanism by which rhACE2 blocks viral infection and analyze the preventive ability of rhACE2 against SARS-CoV-2 and the effectiveness of therapies for COVID-19. This technique is expected to provide an effective analytical method for quantifying the dynamic distribution of rhACE2 *in vivo* and a scientific basis for the effectiveness of rhACE2 therapy.

The most prominent symptom of SARS-CoV-2 infection is respiratory tract infection, but much evidence shows that the virus can cause multisystem damage. Acute kidney injury (AKI) is one of the most common and serious organ complications of novel coronavirus<sup>8</sup>. IHC staining showed high expression of ACE2 in the kidney. PET images also showed the super uptake of probe in the kidney. Although the high uptake of the kidneys is partly because the kidneys are the metabolic organs of the probe, after subcutaneous injection of 0.4 nmol rhACE2, HZ20 blocking and nonblocking studies showed that the kidneys do have a high specific uptake of the probe, and the SUVmax of the kidneys 60 min after probe injection was  $3.81 \pm 0.32$  to  $4.92 \pm 0.05$  ( $P=0.004$ ). This demonstrates the high expression of ACE2 in the kidneys, which partly supports AKI caused by SARS-CoV-2 infection.

Approximately one-fifth of patients suffer from liver injury during SARS-CoV-2 infection, and the incidence of liver decompensation and acute and chronic liver failure is higher in patients with liver cirrhosis<sup>10,35–37</sup>. Our <sup>68</sup>Ga-HZ20 probe can be used to accurately locate and quantify rhACE2 in the liver to provide support for the prevention of serious liver complications by exogenous ACE2.

The virus may accumulate in the olfactory bulb and vagus nerve through the blood brain barrier (BBB) to infiltrate the central nervous system (CNS)<sup>38,39</sup>. Some studies have confirmed the existence of SARS-CoV-2 in the brain and cerebrospinal fluid<sup>40</sup>. A recent meta-analysis report showed that more than 40% of patients had psychiatric and neuropsychiatric symptoms associated with severe coronavirus infection at an early stage<sup>39,41–46</sup>. We injected rhACE2 into the anterior fontanel of the mouse brain at a fixed point. PET imaging demonstrated that <sup>68</sup>Ga-HZ20 can reach brain tissue, target lesions at fixed points, and detect changes in rhACE2, which supports its use in monitoring rhACE2 changes in the brain.

ACE2 is highly expressed in many tumors and is a potential protective factor against cancer progression<sup>3,11,47</sup>. However, as the host cell receptor of SARS-CoV-2, the high expression of ACE2 may increase the risk of SARS-CoV-2 infection<sup>35,48</sup>. Studies have found that the SARS-CoV-2 spike protein not only binds to ACE2 to mediate infection of host cells but also activates intracellular signals to degrade ACE2 mRNA after entering host cells. After downregulation of ACE2 expression in infected cells, the level of angiotensin II increases. High-dose angiotensin II induces the death of arterial endothelial cells and exacerbates cardiovascular disease<sup>49</sup>. Therefore, it may not be a wise choice to use ACE2 inhibitors to prevent and treat COVID-19. For tumor patients, rhACE2 may be a reliable therapy. The <sup>68</sup>Ga-HZ20 probe can also be used to monitor the tumor site of these patients, and exogenous infusion of rhACE2 can help achieve more precise treatment.

Based on the positive correlation between the uptake value of the probe SUVmax and the content of rhACE2 as well as the precise positioning ability of the probe at the target site, PET imaging can be used for noninvasive real-time quantification of the content and spatial distribution of the receptor, which provides scientific guidance for the formulation of prevention and treatment measures for SARS-CoV-2.

## Ethical Statement

All animal studies were performed according to a protocol approved by the Peking University Cancer Hospital Animal Care and in accordance with the ethical standards of the Declaration of Helsinki. Protocol Number EAEC 2022-01.

## Acknowledgments

This study was supported by Beijing Hospitals Authority Dengfeng Project (DFL20191102), The Pilot Project (4<sup>th</sup> Round) to Reform Public Development of Beijing Municipal Medical Research Institute (2021-1), the Shenzhen Science and Technology Program (1210318663) and the third foster plan in 2019 "Molecular Imaging Probe Preparation and Characterization of Key Technologies and Equipment" for the development of key technologies and equipment in major science and technology infrastructure in Shenzhen.

### Author Contributions

Youping Liu, Hua Zhu and Qi Liu conceived and designed this research. Zilei Wang, Chuanke Zhao and Chuangui Li performed experiments, data collection and analysis, and wrote the manuscript. Song Liu, Jin Ding, Chengxue He and Jiayue Liu were involved in the preparation of radiopharmaceuticals and took part in most of the animal experiments and responsible for part data analysis. Bin Dong and Zhi Yang participated the approving the manuscript.

### Conflicts of Interest

The authors declare that there is no conflict of interest regarding the publication of this article.

### Data Availability

All data in this study are available from the corresponding author upon reasonable request.

### References

1. Datta PK, Liu F, Fischer T, Rappaport J, Qin X. SARS-CoV-2 pandemic and research gaps: Understanding SARS-CoV-2 interaction with the ACE2 receptor and implications for therapy. *Theranostics* 2020; 10: 7448–64.
2. Zhou P, Yang X-L, Wang X-G, Hu B, Zhang L, Zhang W, Si H-R, Zhu Y, Li B, Huang C-L, Chen H-D, Chen J, Luo Y, Guo H, Jiang R-D, Liu M-Q, Chen Y, Shen X-R, Wang X, Zheng X-S, Zhao K, Chen Q-J, Deng F, Liu L-L, Yan B, Zhan F-X, Wang Y-Y, Xiao G-F, Shi Z-L. A pneumonia outbreak associated with a new coronavirus of probable bat origin. *Nature* 2020; 579: 270–3.
3. Yang J, Li H, Hu S, Zhou Y. ACE2 correlated with immune infiltration serves as a prognostic biomarker in endometrial carcinoma and renal papillary cell carcinoma: implication for COVID-19. *Aging* 2020; 12: 6518–35.
4. Gheblawi M, Wang K, Viveiros A, Nguyen Q, Zhong J-C, Turner AJ, Raizada MK, Grant MB, Oudit GY. Angiotensin-Converting Enzyme 2: SARS-CoV-2 Receptor and Regulator of the Renin-Angiotensin System: Celebrating the 20th Anniversary of the Discovery of ACE2. *Circ Res* 2020; 126: 1456–74.
5. Li Y, Zhou W, Yang L, You R. Physiological and pathological regulation of ACE2, the SARS-CoV-2 receptor. *Pharmacol Res* 2020; 157: 104833.
6. Patel VB, Zhong J-C, Grant MB, Oudit GY. Role of the ACE2/Angiotensin 1-7 Axis of the Renin-Angiotensin System in Heart Failure. *Circ Res* 2016; 118: 1313–26.
7. Burrell LM, Johnston CI, Tikellis C, Cooper ME. ACE2, a new regulator of the renin-angiotensin system. *Trends Endocrinol Metab* 2004; 15: 166–9.
8. Chávez-Valencia V, Orizaga-de-la-Cruz C, Lagunas-Rangel FA. Acute Kidney Injury in COVID-19 Patients: Pathogenesis, Clinical Characteristics, Therapy, and Mortality. *Dis Basel Switz* 2022; 10: 53.
9. Verdecchia P, Cavallini C, Spanevello A, Angeli F. The pivotal link between ACE2 deficiency and SARS-CoV-2 infection. *Eur J Intern Med* 2020; 76: 14–20.
10. Marjot T, Webb GJ, Barritt AS, Moon AM, Stamataki Z, Wong VW, Barnes E. COVID-19 and liver disease: mechanistic and clinical perspectives. *Nat Rev Gastroenterol Hepatol* 2021; 18: 348–64.

11. Zhang Z, Li L, Li M, Wang X. The SARS-CoV-2 host cell receptor ACE2 correlates positively with immunotherapy response and is a potential protective factor for cancer progression. *Comput Struct Biotechnol J* 2020; 18: 2438–44.
12. Kyriakidis NC, López-Cortés A, González EV, Grimaldos AB, Prado EO. SARS-CoV-2 vaccines strategies: a comprehensive review of phase 3 candidates. *NPJ Vaccines* 2021; 6: 28.
13. Harvey WT, Carabelli AM, Jackson B, Gupta RK, Thomson EC, Harrison EM, Ludden C, Reeve R, Rambaut A, COVID-19 Genomics UK (COG-UK) Consortium, Peacock SJ, Robertson DL. SARS-CoV-2 variants, spike mutations and immune escape. *Nat Rev Microbiol* 2021; 19: 409–24.
14. Garcia-Beltran WF, Lam EC, St Denis K, Nitido AD, Garcia ZH, Hauser BM, Feldman J, Pavlovic MN, Gregory DJ, Poznansky MC, Sigal A, Schmidt AG, Iafrate AJ, Naranbhai V, Balazs AB. Multiple SARS-CoV-2 variants escape neutralization by vaccine-induced humoral immunity. *Cell* 2021; 184: 2372-2383.e9.
15. Cele S, Gazy I, Jackson L, Hwa S-H, Tegally H, Lustig G, Giandhari J, Pillay S, Wilkinson E, Naidoo Y, Karim F, Ganga Y, Khan K, Bernstein M, Balazs AB, Gosnell BI, Hanekom W, Moosa M-YS, Network for Genomic Surveillance in South Africa, COMMIT-KZN Team, Lessells RJ, de Oliveira T, Sigal A. Escape of SARS-CoV-2 501Y.V2 from neutralization by convalescent plasma. *Nature* 2021; 593: 142–6.
16. Cao Y, Wang J, Jian F, Xiao T, Song W, Yisimayi A, Huang W, Li Q, Wang P, An R, Wang J, Wang Y, Niu X, Yang S, Liang H, Sun H, Li T, Yu Y, Cui Q, Liu S, Yang X, Du S, Zhang Z, Hao X, Shao F, Jin R, Wang X, Xiao J, Wang Y, Xie XS. Omicron escapes the majority of existing SARS-CoV-2 neutralizing antibodies. *Nature* 2022; 602: 657–63.
17. Planas D, Veyer D, Baidaliuk A, Staropoli I, Guivel-Benhassine F, Rajah MM, Planchais C, Porrot F, Robillard N, Puech J, Prot M, Gallais F, Gantner P, Velay A, Le Guen J, Kassis-Chikhani N, Edriss D, Belec L, Seve A, Courtellemont L, Péré H, Hocqueloux L, Fafi-Kremer S, Prazuck T, Mouquet H, Bruel T, Simon-Lorière E, Rey FA, Schwartz O. Reduced sensitivity of SARS-CoV-2 variant Delta to antibody neutralization. *Nature* 2021; 596: 276–80.
18. Greaney AJ, Starr TN, Barnes CO, Weisblum Y, Schmidt F, Caskey M, Gaebler C, Cho A, Agudelo M, Finkin S, Wang Z, Poston D, Muecksch F, Hatziioannou T, Bieniasz PD, Robbiani DF, Nussenzweig MC, Bjorkman PJ, Bloom JD. Mapping mutations to the SARS-CoV-2 RBD that escape binding by different classes of antibodies. *Nat Commun* 2021; 12: 4196.
19. Lopez Bernal J, Andrews N, Gower C, Gallagher E, Simmons R, Thelwall S, Stowe J, Tessier E, Groves N, Dabrera G, Myers R, Campbell CNJ, Amirthalingam G, Edmunds M, Zambon M, Brown KE, Hopkins S, Chand M, Ramsay M. Effectiveness of Covid-19 Vaccines against the B.1.617.2 (Delta) Variant. *N Engl J Med* 2021; 385: 585–94.
20. Takashita E, Kinoshita N, Yamayoshi S, Sakai-Tagawa Y, Fujisaki S, Ito M, Iwatsuki-Horimoto K, Chiba S, Halfmann P, Nagai H, Saito M, Adachi E, Sullivan D, Pekosz A, Watanabe S, Maeda K, Imai M, Yotsuyanagi H, Mitsuya H, Ohmagari N, Takeda M, Hasegawa H, Kawaoka Y. Efficacy of Antibodies and Antiviral Drugs against Covid-19 Omicron Variant. *N Engl J Med* 2022; 386: 995–8.
21. Peng Q, Zhou R, Wang Y, Zhao M, Liu N, Li S, Huang H, Yang D, Au K-K, Wang H, Man K, Yuen K-Y, Chen Z. Waning immune responses against SARS-CoV-2 variants of concern among vaccinees in Hong Kong. *EBioMedicine* 2022; 77: 103904.
22. Gaziano L, Giambartolomei C, Pereira AC, Gaulton A, Posner DC, Swanson SA, Ho Y-L, Iyengar SK, Kosik NM, Vujkovic M, Gagnon DR, Bento AP, Barrio-Hernandez I, Rönnblom L, Hagberg N, Lundtoft C, Langenberg C, Pietzner M, Valentine D, Gustincich S, Tartaglia GG, Allara E, Surendran P, Burgess S, Zhao JH, Peters JE, Prins BP, Angelantonio ED, Devineni P, Shi Y, Lynch KE, DuVall SL, Garcon H, Thomann LO, Zhou JJ, Gorman BR, Huffman JE, O'Donnell CJ, Tsao PS, Beckham JC, Pyarajan S, Muralidhar S, Huang GD, Ramoni R, Beltrao P, Danesh J, Hung AM, Chang K-M, Sun YV, Joseph J, Leach

- AR, Edwards TL, Cho K, Gaziano JM, Butterworth AS, Casas JP, VA Million Veteran Program COVID-19 Science Initiative. Actionable druggable genome-wide Mendelian randomization identifies repurposing opportunities for COVID-19. *Nat Med* 2021; 27: 668–76.
23. Linsky TW, Vergara R, Codina N, Nelson JW, Walker MJ, Su W, Barnes CO, Hsiang T-Y, Esser-Nobis K, Yu K, Reneer ZB, Hou YJ, Priya T, Mitsumoto M, Pong A, Lau UY, Mason ML, Chen J, Chen A, Berrocal T, Peng H, Clairmont NS, Castellanos J, Lin Y-R, Josephson-Day A, Baric RS, Fuller DH, Walkey CD, Ross TM, Swanson R, Bjorkman PJ, Gale M, Blancas-Mejia LM, Yen H-L, Silva D-A. De novo design of potent and resilient hACE2 decoys to neutralize SARS-CoV-2. *Science* 2020; 370: 1208–14.
24. Higuchi Y, Suzuki T, Arimori T, Ikemura N, Mihara E, Kirita Y, Ohgitani E, Mazda O, Motooka D, Nakamura S, Sakai Y, Itoh Y, Sugihara F, Matsuura Y, Matoba S, Okamoto T, Takagi J, Hoshino A. Engineered ACE2 receptor therapy overcomes mutational escape of SARS-CoV-2. *Nat Commun* 2021; 12: 3802.
25. Imai Y, Kuba K, Rao S, Huan Y, Guo F, Guan B, Yang P, Sarao R, Wada T, Leong-Poi H, Crackower MA, Fukamizu A, Hui C-C, Hein L, Uhlig S, Slutsky AS, Jiang C, Penninger JM. Angiotensin-converting enzyme 2 protects from severe acute lung failure. *Nature* 2005; 436: 112–6.
26. Monteil V, Kwon H, Prado P, Hagelkrüys A, Wimmer RA, Stahl M, Leopoldi A, Garreta E, Hurtado Del Pozo C, Prosper F, Romero JP, Wirnsberger G, Zhang H, Slutsky AS, Conder R, Montserrat N, Mirazimi A, Penninger JM. Inhibition of SARS-CoV-2 Infections in Engineered Human Tissues Using Clinical-Grade Soluble Human ACE2. *Cell* 2020; 181: 905-913.e7.
27. Monteil V, Eaton B, Postnikova E, Murphy M, Braunsfeld B, Crozier I, Kricek F, Niederhöfer J, Schwarzböck A, Breid H, Devignot S, Klingström J, Thälín C, Kellner MJ, Christ W, Havervall S, Me-reiter S, Knapp S, Sanchez Jimenez A, Bugajska-Schretter A, Dohnal A, Ruf C, Gugenberger R, Hagelkruys A, Montserrat N, Koziaradzki I, Hasan Ali O, Stadlmann J, Holbrook MR, Schmaljohn C, Oostenbrink C, Shoemaker RH, Mirazimi A, Wirnsberger G, Penninger JM. Clinical grade ACE2 as a universal agent to block SARS-CoV-2 variants. *EMBO Mol Med* 2022; 14: e15230.
28. Shoemaker RH, Panettieri RA, Libutti SK, Hochster HS, Watts NR, Wingfield PT, Starkl P, Pimenov L, Gawish R, Hladik A, Knapp S, Boring D, White JM, Lawrence Q, Boone J, Marshall JD, Matthews RL, Cholewa BD, Richig JW, Chen BT, McCormick DL, Gugensberger R, Höller S, Penninger JM, Wirnsberger G. Development of an aerosol intervention for COVID-19 disease: Tolerability of soluble ACE2 (APN01) administered via nebulizer. *PloS One* 2022; 17: e0271066.
29. South AM, Diz DI, Chappell MC. COVID-19, ACE2, and the cardiovascular consequences. *Am J Physiol Heart Circ Physiol* 2020; 318: H1084–90.
30. Khanna A, English SW, Wang XS, Ham K, Tumlin J, Szerlip H, Busse LW, Altaweel L, Albertson TE, Mackey C, McCurdy MT, Boldt DW, Chock S, Young PJ, Krell K, Wunderink RG, Ostermann M, Murugan R, Gong MN, Panwar R, Hästbacka J, Favory R, Venkatesh B, Thompson BT, Bellomo R, Jensen J, Kroll S, Chawla LS, Tidmarsh GF, Deane AM, ATHOS-3 Investigators. Angiotensin II for the Treatment of Vasodilatory Shock. *N Engl J Med* 2017; 377: 419–30.
31. Huang L, Sexton DJ, Skogerson K, Devlin M, Smith R, Sanyal I, Parry T, Kent R, Enright J, Wu Q, Conley G, DeOliveira D, Morganelli L, Ducar M, Wescott CR, Ladner RC. Novel peptide inhibitors of angiotensin-converting enzyme 2. *J Biol Chem* 2003; 278: 15532–40.
32. Zhu H, Zhang H, Zhou N, Ding J, Jiang J, Liu T, Liu Z, Wang F, Zhang Q, Zhang Z, Yan S, Li L, Benabdallah N, Jin H, Liu Z, Cai L, Thorek DLJ, Yang X, Yang Z. Molecular PET/CT Profiling of ACE2 Expression In Vivo: Implications for Infection and Outcome from SARS-CoV-2. *Adv Sci Weinh Baden-Wurt Ger* 2021; 8: e2100965.
33. Liu S, Li G, Ding L, Ding J, Zhang Q, Li D, Hou X, Kong X, Zou J, Zhang S, Han H, Wan Y, Yang Z, Zhu H. Evaluation of SARS-CoV-2-Neutralizing Nanobody Using Virus Receptor Binding Domain-Administered

Model Mice. *Res Wash DC* 2022; 2022: 9864089.

34. Brevini T, Maes M, Webb GJ, John BV, Fuchs CD, Buescher G, Wang L, Griffiths C, Brown ML, Scott WE, Pereyra-Gerber P, Gelson WTH, Brown S, Dillon S, Muraro D, Sharp J, Neary M, Box H, Tatham L, Stewart J, Curley P, Pertinez H, Forrest S, Mlcochova P, Varankar SS, Darvish-Damavandi M, Mulcahy VL, Kuc RE, Williams TL, Heslop JA, Rossetti D, Tysoe OC, Galanakis V, Vila-Gonzalez M, Crozier TWM, Bargehr J, Sinha S, Upponi SS, Fear C, Swift L, Saeb-Parsy K, Davies SE, Wester A, Hagström H, Melum E, Clements D, Humphreys P, Herriott J, Kijak E, Cox H, Bramwell C, Valentijn A, Illingworth CJR, UK-PBC research consortium, Dahman B, Bastaich DR, Ferreira RD, Marjot T, Barnes E, Moon AM, Barritt AS, Gupta RK, Baker S, Davenport AP, Corbett G, Gorgoulis VG, Buczacki SJA, Lee J-H, Matheson NJ, Trauner M, Fisher AJ, Gibbs P, Butler AJ, Watson CJE, Mells GF, Dougan G, Owen A, Lohse AW, Vallier L, Sampaziotis F. FXR inhibition may protect from SARS-CoV-2 infection by reducing ACE2. *Nature* 2022 Dec 5. doi: 10.1038/s41586-022-05594-0
35. An X, Lin W, Liu H, Zhong W, Zhang X, Zhu Y, Wang X, Li J, Sheng Q. SARS-CoV-2 Host Receptor ACE2 Protein Expression Atlas in Human Gastrointestinal Tract. *Front Cell Dev Biol* 2021; 9: 659809.
36. Iwasaki M, Saito J, Zhao H, Sakamoto A, Hirota K, Ma D. Inflammation Triggered by SARS-CoV-2 and ACE2 Augment Drives Multiple Organ Failure of Severe COVID-19: Molecular Mechanisms and Implications. *Inflammation* 2021; 44: 13–34.
37. Gracia-Ramos AE, Jaquez-Quintana JO, Contreras-Omaña R, Auron M. Liver dysfunction and SARS-CoV-2 infection. *World J Gastroenterol* 2021; 27: 3951–70.
38. Wu Y, Xu X, Chen Z, Duan J, Hashimoto K, Yang L, Liu C, Yang C. Nervous system involvement after infection with COVID-19 and other coronaviruses. *Brain Behav Immun* 2020; 87: 18–22.
39. Liguori C, Pierantozzi M, Spanetta M, Sarmati L, Cesta N, Iannetta M, Ora J, Mina GG, Puxeddu E, Balbi O, Pezzuto G, Magrini A, Rogliani P, Andreoni M, Mercuri NB. Subjective neurological symptoms frequently occur in patients with SARS-CoV2 infection. *Brain Behav Immun* 2020; 88: 11–6.
40. Paterson RW, Brown RL, Benjamin L, Nortley R, Wiethoff S, Bharucha T, Jayaseelan DL, Kumar G, Raftopoulos RE, Zambreau L, Vivekanandam V, Khoo A, Geraldine R, Chinthapalli K, Boyd E, Tuzlali H, Price G, Christofi G, Morrow J, McNamara P, McLoughlin B, Lim ST, Mehta PR, Levee V, Keddie S, Yong W, Trip SA, Foulkes AJM, Hotton G, Miller TD, Everitt AD, Carswell C, Davies NWS, Yoong M, Attwell D, Sreedharan J, Silber E, Schott JM, Chandratheva A, Perry RJ, Simister R, Checkley A, Longley N, Farmer SF, Carletti F, Houlihan C, Thom M, Lunn MP, Spillane J, Howard R, Vincent A, Werring DJ, Hoskote C, Jäger HR, Manji H, Zandi MS. The emerging spectrum of COVID-19 neurology: clinical, radiological and laboratory findings. *Brain J Neurol* 2020; 143: 3104–20.
41. Rogers JP, Chesney E, Oliver D, Pollak TA, McGuire P, Fusar-Poli P, Zandi MS, Lewis G, David AS. Psychiatric and neuropsychiatric presentations associated with severe coronavirus infections: a systematic review and meta-analysis with comparison to the COVID-19 pandemic. *Lancet Psychiatry* 2020; 7: 611–27.
42. Moldofsky H, Patcai J. Chronic widespread musculoskeletal pain, fatigue, depression and disordered sleep in chronic post-SARS syndrome; a case-controlled study. *BMC Neurol* 2011; 11: 37.
43. Guedj E, Million M, Dudouet P, Tissot-Dupont H, Bregeon F, Cammilleri S, Raoult D. 18F-FDG brain PET hypometabolism in post-SARS-CoV-2 infection: substrate for persistent/delayed disorders? *Eur J Nucl Med Mol Imaging* 2021; 48: 592–5.
44. de Paula JJ, Paiva RERP, Souza-Silva NG, Rosa DV, Duran FL de S, Coimbra RS, Costa D de S, Dutenhofner PR, Oliveira HSD, Camargos ST, Vasconcelos HMM, de Oliveira Carvalho N, da Silva JB, Silveira MB, Malamut C, Oliveira DM, Molinari LC, de Oliveira DB, Januário JN, Silva LC, De Marco LA, Queiroz DM de M, Meira W, Busatto G, Miranda DM, Romano-Silva MA. Selective visuocognitive impairment following mild COVID-19 with inflammatory and neuroimaging correlation findings. *Mol Psychiatry* 2022; 1–11.

45. Rudroff T, Workman CD, Ponto LLB. 18F-FDG-PET Imaging for Post-COVID-19 Brain and Skeletal Muscle Alterations. *Viruses* 2021; 13: 2283.
46. Hosp JA, Dressing A, Blazhenets G, Bormann T, Rau A, Schwabenland M, Thurow J, Wagner D, Waller C, Niesen WD, Frings L, Urbach H, Prinz M, Weiller C, Schroeter N, Meyer PT. Cognitive impairment and altered cerebral glucose metabolism in the subacute stage of COVID-19. *Brain J Neurol* 2021; 144: 1263–76.
47. Zhang Q, Lu S, Li T, Yu L, Zhang Y, Zeng H, Qian X, Bi J, Lin Y. ACE2 inhibits breast cancer angiogenesis via suppressing the VEGFa/VEGFR2/ERK pathway. *J Exp Clin Cancer Res CR* 2019; 38: 173.
48. Chai P, Yu J, Ge S, Jia R, Fan X. Genetic alteration, RNA expression, and DNA methylation profiling of coronavirus disease 2019 (COVID-19) receptor ACE2 in malignancies: a pan-cancer analysis. *J Hematol OncolJ Hematol Oncol* 2020; 13: 43.
49. Kuba K, Imai Y, Rao S, Gao H, Guo F, Guan B, Huan Y, Yang P, Zhang Y, Deng W, Bao L, Zhang B, Liu G, Wang Z, Chappell M, Liu Y, Zheng D, Leibbrandt A, Wada T, Slutsky AS, Liu D, Qin C, Jiang C, Penninger JM. A crucial role of angiotensin converting enzyme 2 (ACE2) in SARS coronavirus-induced lung injury. *Nat Med* 2005; 11: 875–9.

### Hosted file

rhACE2-Figure.pptx available at <https://authorea.com/users/615871/articles/642083-molecular-pet-ct-mapping-of-rhace2-distribution-and-quantification-in-organs-to-aid-in-sars-cov-2-targeted-therapy>